RSC Advances

ROYAL SOCIETY OF CHEMISTRY

www.rsc.org/advances

A combined H_3PO_4 activation and boron templating process for facile synthesis of highly porous spherical activated carbons as superior adsorbent for rhodamine B

Zhimin Zou,[a,b] Yong Zhang,[b] Houan Zhang,[b] Chunhai Jiang,[a,b,*]

[a] Institute of Advanced Energy Materials, School of Materials Science and Engineering, Xiamen University of Technology, 600 Ligong Road, Jimei District, Xiamen 361024, Fujian, China

[b] School of Materials Science and Engineering, Xiamen University of Technology, 600 Ligong Road, Jimei District, Xiamen 361024, Fujian, China

Abstract

Spherical activated carbons (SACs) with a high surface area of 2729 m^2 g^{-1} and a large total pore volume of 1.529 cm^3 g^{-1} were facilely prepared by phosphoric acid activation of boron incorporated polymeric precursor followed by washing off the in situ formed BPO_4 with base solution. The reaction induced extraction of the pre-embedded boron from the carbon matrix produced additional pores, which greatly improved the texture properties of the obtained SACs. As was tested as an adsorbent for bulky rhodamine B molecular, the SACs exhibited extremely high adsorption capability up to 833 mg g^{-1} at ambient temperature and at an adsorbent dosage of 1 g L^{-1}. The adsorption isotherms and kinetics data were well fitted by the Langmuir isotherm model and pseudo-second-order kinetic model, respectively, suggestive of formation of rhodamine B monolayer on the SACs possibly through chemical interactions such as ionic or covalent bonds.

* Corresponding author

E-mail: chjiang@xmut.edu.cn

Tel. & Fax: +86-592 6291693

Keywords: Spherical activated carbons; H_3PO_4 activation; Texture properties; Dye removal; Rhodamine B

1. Introduction

Activated carbons are very important functional materials that have been intimately applied in our daily lives like air and water purification, food and beverage industries, medical treatments, energy storage, and so on [1]. The property of activated carbons depends greatly on their specific surface area, pore volume and pore size distribution, the amount and types of surface functional groups. Besides that, the geometrical shapes of activated carbons are also important factors that have to be considered before applications. As compared to granular and powdered activated carbons, spherical activated carbons (SACs) have displayed distinguished advantages including controllable sizes, high wear resistance, good fluidity, high packaging density, and good adsorption performance [2, 3]. These merits have brought out SACs for wide applications in blood purification [4], catalyst supports [5-7], gas storage [2, 8], drug delivery [9], adsorbents [10-12], and electrode of supercapacitors [13-15]. Due to these promising properties and applications, development of SACs with extended surface areas and tailored texture properties have been always the interests of many researchers [16, 17].

Preparation of SACs normally involves the fabrication of spherical precursors and post-synthesis activation process. Various materials including coal [18], petroleum pitch [19], phenolic-resin [20-23], lignocellulosic biomasses [24-27], carbohydrates [3, 28, 29] and natural biomass [14, 15], have been used to synthesize spherical carbon precursors.

Among them, phenolic-resin based polymeric spheres prepared from various reaction systems like resorcinol–formaldehyde [30, 31], urea–formaldehyde [32], melamine–formaldehyde [33, 34], and resorcinol–hexamethylenetetramine [35] using the extended Stöber method have been extensively investigated considering the high purity, well controlled particle sizes and high yield of carbon products [36]. Post-synthesis activation of the carbon precursors can be carried out both physically by CO_2 and steam or chemically by $ZnCl_2$, H_3PO_4, KOH, and NaOH. Physical activations normally produce microporosity dominant activated carbons. Extending the degree of activation by elevating the activation temperature and/or elongating the activation time may effectively improve the surface area and pore volume but is always on the costs of decreased carbon yield and mechanical strength [8, 30]. By contrast, chemical activation can not only produce a large development of microporosity, but also develop large mesopores and even macropores while maintaining a high carbon yield, especially when $ZnCl_2$ and H_3PO_4 are used as the activating agents [37-39]. In this sense, chemical activation has been preferably adopted to prepare SACs for the applications where a certain portion of mesopores or macropores is necessitous to promote the mass transfer within the activated carbons, such as adsorption of bulky dyes [11, 39, 40] and electrode of supercapacitors using organic electrolytes [41].

Combination of post-synthesis activation and salt templating has recently emerged as another effective technique to tune the texture properties of activated carbons [31, 42-48]. The carbon precursors incorporated by or impregnated with salts are carbonized at an elevated temperature, followed by washing off the salt nano-clusters to produce

additional pores. For example, Antonietti et al. synthesized porous triazine-based materials with high surface area by using molten $ZnCl_2$ as an activating agent and also as a catalyst for the polymerization reaction [47, 48]. Ludwinowicz and Jaroniec directly incorporated potassium oxalate into phenolic-resin spheres during the polymerization process of resorcinol and formaldehyde and treated it as the activating agent in the subsequent carbonization process [31]. By further washing off the inorganic residual with diluted HCl solution, SACs with a surface area of 2130 $m^2 g^{-1}$ and a total pore volume of 1.10 $cm^3 g^{-1}$ were obtained [31].

Inspired by these aforementioned works, we speculate that the salt templating technique can be well combined with the conventional chemical activating process to tune the texture properties of porous carbons upon the previously incorporated elements in carbon precursors can be easily extracted out by the activating agents via formation of soluble inorganic salts. Saying this, phosphoric acid is an especially ideal chemical activating agent in comparison to $ZnCl_2$ and KOH as PO_4^{3-} is not volatile and can form a large number of alkaline or acid soluble phosphates with elements like Fe, Ni, B and others that can be incorporated into carbon precursors [49-51].

To verify the above speculation, herein we report a facile process for preparation of SACs with much improved texture properties through phosphoric acid activation of boron incorporated phenolic-resin microspheres followed by washing off the in situ formed boron phosphate (BPO_4) with basic solution. SACs with a high surface area of 2729 $m^2 g^{-1}$ and a large total pore volume of 1.529 $cm^3 g^{-1}$ was prepared by this method, and when being tested as an adsorbent for bulky organic dye, the SACs exhibited very

high adsorption capability as well as fast adsorption kinetics towards rhodamine B.

2. Experimental details

2.1 Chemicals

Analytical grade resorcinol (R, $C_6H_6O_2$, 99.5 wt.%), hexamethylenetetramine (HMT, $C_6H_{12}N_4$, 99 wt.%), boric acid (H_3BO_3, 99.5 wt.%), phosphoric acid (H_3PO_4, 85 wt.% in water), hydrochloride acid (HCl, 35-37 wt.%), sodium hydroxide (NaOH, 99 wt.%) and rhodamine B (RB, $C_{28}H_{31}ClN_2O_3$, 99.5 wt.%) were purchased from Sinopharm Chemical Reagent Co. Ltd and used as received. Deionized water was used throughout the experiments as solvent and cleaning media.

2.2 Synthesis and characterizations of SACs

The spherical activated carbons with high surface area and large pore volume were prepared by phosphoric acid activation of boron incorporated phenolic-resin spheres synthesized by a modified Stöber method and followed by base leaching. In a typical process, 10 g resorcinol, 4 g boric acid, and 4.2 g HMT were dissolved completely in 60 ml deionized water with heating at 60^{o}C for 10 min under magnetic stirring. The solution was transferred into a 100 ml Teflon-line stainless steel autoclave, sealed and held at 140^{o}C for 4 h. The obtained colloid suspension was directly dried at 60^{o}C in a petri dish for a few hours followed by simple grinding with an agate mortar and pestle to yield well dispersed boron-incorporated phenolic-resin microspheres. To perform the chemical activation, two batches (10 g/batch) of the obtained spherical polymeric powders were mixed with 30 or 40 g phosphoric acid (85 wt.%) in 40 ml water, respectively. The mixtures were magnetically stirred for 12 h at ambient temperature to

get the organic spheres being completely impregnated by phosphoric acid. After that, the mixtures were dried in an oven first at 60°C for 12 h and then at 120°C for 6 h. Carbonization and activation of the dried mixtures were performed in a horizontal tube furnace at 500 or 600°C for 1 h under flowing high purity argon (99.99%). The carbonized powders were washed by 1 M HCl solution first and then 2 M NaOH solution with intermediate filtration and drying. Heating of the base solution was conducted to better remove the in situ formed BPO_4 from the porous carbon spheres. To simplify the description, the samples were named as 1v3-T, 1v3-TN, 1v4-T, and 1v4-TN, respectively, where T represented the activation temperature and N indicated the sample leached by NaOH solution. For example, 1v3-500 and 1v3-500N referred to the samples activated with 3 times of weight ratio of phosphoric acid to carbon precursors at 500°C, before and after base leaching with NaOH, respectively.

The microstructures of the obtained SACs were examined by scanning electron microscopy (SEM, FEI F50) and X-ray diffraction (D/Max-2500PC) methods. Nitrogen adsorption/desorption isotherms were measured with a surface area and porosimetry analyzer V-sorb 2800P at 77 K. The specific surface areas were calculated according to the Brunauer–Emmert–Teller (BET) method [52]. The total pore volumes (V_t) were calculated from the amount of adsorbed nitrogen at a relative pressure, P/P_0, of 0.99 [53]. The micropore volumes (V_{micro}) were calculated using *t*-plot method. Pore size distributions were determined from the adsorption branches of the isotherms using the quenched solid density functional theory (QSDFT) provided by Quantachrome software. The mass ratios of carbon and BPO_4 in the phosphoric acid activated and acid washed

powders were estimated by thermal gravimetric analysis (TGA, Shimadzu DTG-60H) performed in flowing air.

2.3 Adsorption of rhodamine B

A batch model was used to examine the adsorption performance of the as-prepared SACs towards RB in 100 mL glass conical flasks containing 20 mL aqueous solution. For detail, 20 mg of SACs was added into RB solutions with varied initial concentrations (100, 200, 300, 400, 500, 600,700, 800 and 1000 mg L^{-1}) without tuning the pH values and agitated at 240 rpm in a rotating bed for 12 h at 25^{o}C. After filtration, the remaining concentrations of RB were measured using an UV-visible spectrometer (Mapada UV-1200, Shanghai) taking 563 nm as the collaboration wavelength. The adsorbed amounts of RB were calculated according to Eq. (1):

$$q_e=(C_0-C_e)V/m \quad (1)$$

where C_0 is the initial concentration, C_e is the equilibrium concentration, V is the volume of the liquid phase and m is the mass of the adsorbent.

To evaluate the adsorption kinetics, 50 mg of the SACs were dispersed in 50 mL of RB solution (400 mg L^{-1}) and agitated at 240 rpm. At certain time intervals, 5 mL of the solution mixture was extracted out and subjected to filtration and RB concentration analysis. The adsorption amounts were calculated following Eq. (2):

$$q_t=(C_0-C_t)V/m \quad (2)$$

where C_0 is the initial concentration, C_t is the remaining concentration at time t, V is the volume of the liquid phase and m is the mass of the SACs. All adsorption experiments were carried out duplicate and the averaged data was presented in this manuscript.

3. Results and discussion

3.1 Microstructure of SACs

Figure 1 shows the typical SEM images of (a) the boron incorporated spheres directly carbonized at 600^{o}C for 2 h, (b) the phosphoric acid activated carbon spheres (1v3-600), (c) the base leached carbon spheres (1v3-600N), and (d) the typical XRD patterns of (i) the phosphoric acid activated carbon spheres (1v3-600) and (ii) that after base leaching (1v3-600N). As can be seen in Fig. 1a, hydrothermal treatment of the mixed aqueous solution of resorcinol, HMT and boric acid had resulted in well confined micron-sized polymer spheres that displayed clean and smooth surface after carbonization. This indicated that boron had been well incorporated into the polymer spheres during the polymerization process. In a preliminary experiment, we found that without addition of boron acid, the polymer spheres would not show highly regular spherical shape. In other words, adding boron acid was beneficial to the formation of well-confined polymeric spheres. After phosphoric acid activation, the spherical morphology of the polymer spheres was preserved (Fig. 1b). Meanwhile, phosphoric acid reacted with the incorporated boron, leading to the formation of BPO_4, which mostly appeared as debris along with the carbon spheres. Base leaching using NaOH solution effectively removed the BPO_4 debris and also possibly that trapped in carbon spheres (Fig. 1c). The XRD patterns shown in Fig. 1d confirmed the formation of a large amount of BPO_4 in the phosphoric acid activated carbon spheres and removal of BPO_4 after NaOH washing.

As was reported, HMT can decompose into NH_3 and formaldehyde [54]. In this

study, the decomposed HMT provided NH_3 as a basic catalyst to catalyze the copolymerization of formaldehyde and resorcinol, forming a resol-type phenolic-resin first, which was then converted to polymeric microspheres via polycondensation under a hydrothermal environment [36]. This result was well consistent with that reported by Sun et al. [35] but with much higher mass loading of the starting reagents and consequently much higher mass production of polymer spheres. Moreover, although incorporation of boron into phenolic-resin using formaldehyde and resorcinol as the carbon precursors and boric acid as the additive has been well conducted [51], a heavy doping of boron in phenolic-resin based polymer spheres presented in this work has not been reported so far.

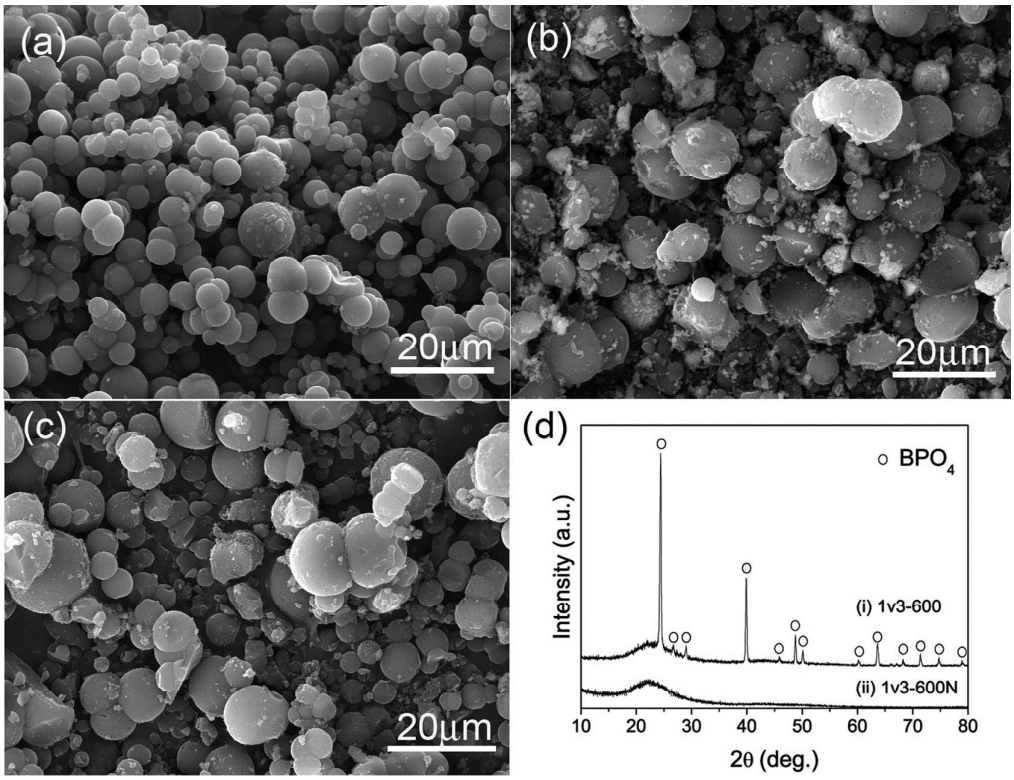

Fig. 1. SEM images of (a) the boron incorporated spheres directly carbonized at 600°C for 2 h, (b) the phosphoric acid activated carbon spheres (1v3-600), (c) the base leached

carbon spheres (1v3-600N), and (d) the typical XRD patterns of (i) the phosphoric acid activated carbon spheres (1v3-600) and (ii) that after base leaching (1v3-600N).

3.2 Texture properties of SACs

The nitrogen adsorption/desorption isotherms and pore size distributions of the selected phosphoric acid activated and base leached samples are given in Fig. 2. The texture properties of the corresponding samples are listed in Table 1. As can be seen from Fig. 2a, all adsorption/desorption isotherms can be categorized to type I according to the IUPAC classification [55], indicating the basically microporous nature of the SACs. However, it is clear to see that the adsorbed nitrogen in all samples gradually increases with the relative pressure (P/P_0) below about 0.4, suggesting the existence of large number of micropores and/or small mesopores in the SACs. In all cases, removing BPO_4 by base leaching has significantly enhanced the nitrogen adsorption capacity of SACs, corresponding to the much improved specific surface areas and pore volumes, as displayed in Table 1. For example, the BET surface areas of samples 1v3-500N, 1v3-600N, and 1v4-600N were increased to 1717, 1865, and 2729 $m^2 g^{-1}$, respectively, from those of samples 1v3-500 (1115 $m^2 g^{-1}$), 1v3-600 (1361 $m^2 g^{-1}$), and 1v4-600 (1419 $m^2 g^{-1}$). Meanwhile, the total pore volumes of samples 1v3-500N, 1v3-600N, and 1v4-600N were 0.912, 0.998, and 1.529 $cm^3 g^{-1}$, respectively, also much higher than those of 1v3-500 (0.630 $cm^3 g^{-1}$), 1v3-600 (0.725 $cm^3 g^{-1}$), and 1v4-600 (0.798 $cm^3 g^{-1}$). This indicated that washing off the BPO_4 both inside and outside the carbon spheres had in one hand improved the carbon purity, in another hand generated additional pores,

both of which had contributed to the increase of the surface area and pore volume. To confirm this speculation, TGA was used to estimate the mass ratio of carbon and BPO_4 in the mixed powders before base leaching. Taking sample 1v4-600 as an instance, the weight percent of carbon in the mixture was about 55.7% (see Fig. S1 in supplementary information). Even assuming the BPO_4 debris in the mixture did not contribute noticeable surface area, the calculated surface area of the carbon spheres after deduction of the weight of BPO_4 was only about 2547 m^2 g^{-1}, still lower than that of 1v4-600N, 2729 m^2 g^{-1}. This suggested that there must be some additional pores generated by BPO_4 removal from inside of the activated carbon spheres. It is noted both from Fig. 2b and Table 1 that, removing BPO_4 did not obviously enlarge the pore diameters within the activated carbon spheres but indeed increased both the micropore and mesopore volumes. In one hand, this increased pore volume could also be partly attributed to the deduction of BPO_4 mass. In another hand, it indicated that the sizes of the in situ formed BPO_4 clusters were not so large to generate large mesopores or macropores. Regarding the effects of impregnation ratios of phosphoric acid to boron incorporated polymer spheres and activating temperatures, the former had played a more important role on the texture development in the base leached SACs. This was reasonable as increasing the amount of phosphoric acid might have not only activated the carbon matrix more sufficiently but extracted the boron from the polymer spheres more completely, which in turn resulted in the much improved pore volume and surface area.

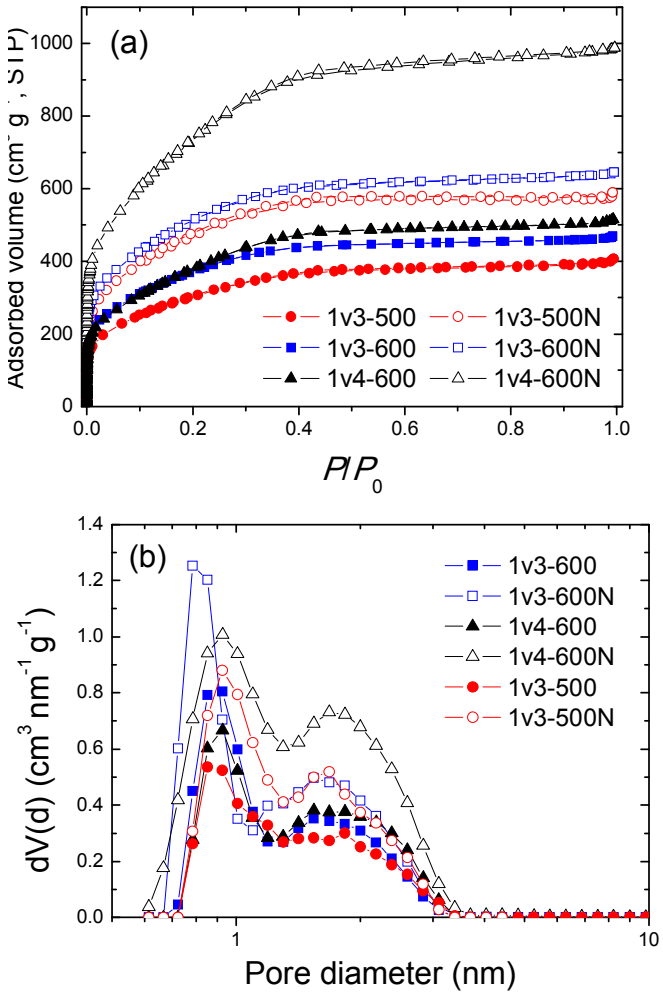

Fig. 2. N_2 adsorption/desorption isotherms (a) and pore diameter distributions (b) of the selected phosphoric acid activated and base leached SACs samples.

Table 1. Texture properties of the SACs before and after base leaching.

Sample	S_{BET} ($m^2\ g^{-1}$)	V_t ($cm^3\ g^{-1}$)	V_{micro} ($cm^3\ g^{-1}$)	V_{micro}/V_t	$D_{average}$ (nm)
1v3-500	1115	0.630	0.355	0.563	2.26
1v3-500N	1717	0.912	0.665	0.729	2.13
1v3-600	1361	0.725	0.521	0.719	2.13

1v3-600N	1854	0.998	0.758	0.760	2.14
1v4-600	1419	0.798	0.364	0.456	2.25
1v4-600N	2729	1.529	0.761	0.498	2.24

S_{BET}: Specific surface area; V_t: single point total pore volume at P/P_0=0.99; V_{micro}:micropore volume obtained by *t*-plot method, $D_{average}$:total adsorption average pore width calculated by $4V_t/S_{BET}$.

3.3 Adsorption property of RB

One typical application of the highly porous SACs is as adsorbent to remove toxic substances from industrial wastewaters. In this work, RB was preliminarily selected as the model bulky dye to evaluate the adsorption ability of the prepared SACs. RB is known as one of the most important dyes within the category of dyestuffs, which has been extensively used as a colorant in the textile and food industries and also as a biological stain in biomedical laboratories [56, 57]. The four *N*-ethyl groups at either side of a xanthene ring in a RB molecular make it toxic and carcinogenic [58]. Therefore, removing RB from industrial effluents is of great importance considering its negative environmental impact.

Figure 3 shows the RB adsorption isotherms measured at 25^{o}C on the obtained SACs before and after base leaching. In general, the equilibrium adsorption amounts of RB on the prepared SACs were consistent with their surface areas and pore volumes. Taking the unleached samples as instances, increasing the activation temperature from 500^{o}C to 600^{o}C was effective in enhancing the RB adsorption capability due to the

obviously improved surface area and pore volume, whereas increasing the impregnation ratio of phosphoric acid to boron incorporated polymer spheres from 3 to 4 did not further improve the surface area and pore volume of the SACs as well as their adsorbed amounts of RB. However, after washing off the BPO_4, not only all the SACs showed significantly enhanced equilibrium adsorption amounts of RB as compared to their unleached counterparts, sample 1v4-600N also exhibited much improved RB removal ability than sample 1v3-600N, consisting well with the greatly enhanced surface area and pore volume in the former.

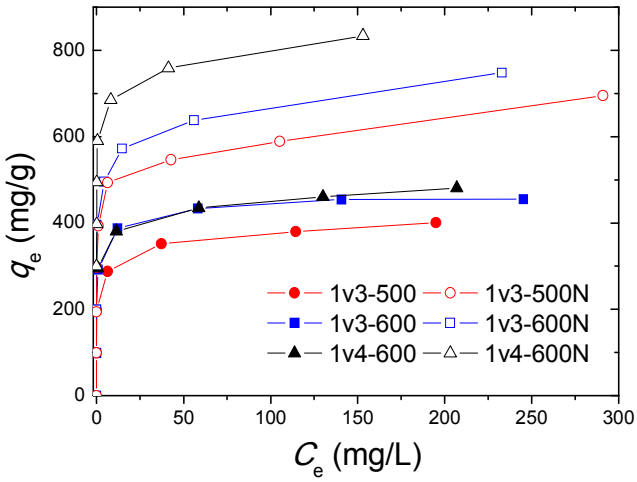

Fig. 3. RB adsorption isotherms measured at 25°C on the obtained SACs before and after base leaching.

To evaluate the maximum adsorption capacities of RB on the prepared SACs as well as to reveal the adsorption mechanism, the equilibrium data were fitted with Langmuir and Freundlich isotherm models by linearly plotting C_e/q_e against C_e (Eq. (3)) [59] and $\ln q_e$ against $\ln C_e$ (eq. 4) [60], respectively.

$$C_e/q_e=k_1/q_m+C_e/q_m \quad (3)$$

$$\ln q_e = \ln k_2 + n^{-1} \ln C_e \quad (4)$$

where C_e is the equilibrium concentration of RB (mg L^{-1}), q_e is the equilibrium adsorption capacity (mg g^{-1}), q_m (mg g^{-1}) and k_1 (L mg^{-1}) are the maximum adsorption capacity and the equilibrium constant of Langmuir model, respectively, and k_2 and n are the constants of Freundlich adsorption. The isotherm parameters obtained from the intercepts and slopes of the linear plots are listed in Table 2.

Table 2. Constants of Langmuir and Freundlich simulations of the RB adsorption isotherms.

Sample	Langmuir isotherm constants			Freundlich isotherm constants		
	k_1 (L mg^{-1})	q_m (mg g^{-1})	R^2	$1/n$ (g L^{-1})	k_2 (mg g^{-1})	R^2
1v3-500	2.164	400	0.998	0.98	241	0.997
1v3-500N	0.647	694	0.994	0.93	555	0.940
1v3-600	0.900	456	0.998	0.80	305	0.956
1v3-600N	0.380	758	0.998	0.91	447	0.989
1v4-600	3.367	483	0.999	0.83	308	0.999
1v4-600N	0.200	833	0.999	0.94	395	0.984

From both the high correlation coefficients (R^2) and the good match between the experimental adsorption capacities and the calculated data, the Langmuir isotherm model was more plausible to describe the adsorption isotherms. In other words, the adsorption of RB on SACs prepared in this study might have occurred by monolayer formation. As can be seen in Table 2, the calculated maximum adsorption amounts of

RB on the base leached SACs ranged from 694 to 833 mg g^{-1}, obviously higher than most reported data achieved on other kinds of activated carbons if the used adsorbent dosage was kept the same, as compared in Table 3. It was well known that a low dosage was helpful to present high adsorption capacity per unit mass of the adsorbent, but likely to lead to low removal efficiency. As shown in Fig. 4, with an adsorbent dosage of 1 g L^{-1}, sample 1v4-600N removed more than 99.9% of the RB when the initial concentrations were lower than or equal to 600 mg L^{-1}. Even at C_0= 700 mg L^{-1}, the removal efficiency was still as high as 98.84%, indicating the very encouraging ability of the prepared SACs for RB removal from aqueous solution. Such a high RB removal efficiency is extremely important for practical applications where complete decoloration of wastewater is specially addressed [61].

Table 3. Comparison of the representative RB adsorption capacities of different activated carbon adsorbents measured at about 25°C.

Adsorbents	S_{BET} (m^2 g^{-1}), V_t (cm^3 g^{-1})	Dosage (g L^{-1})	q_m (mg g^{-1})	Ref.
Activated pyrolytic tire char (APTC)	720, 1.05	0.2	307.2	[62]
Orange peel derived activated carbon	1090, 1.2	0.4	522	[63]
Rice husk-based porous carbons	1803, 3.2	1.0	478.5	[64]

Coconut shell based activated carbons	1947 ± 156, 1.71 ± 0.1	1.0	714	[24]
Ordered mesoporous carbons (MPSC/C)	2580, 2.16	0.4	785	[61]
Glucose derived SACs	2902.5, 1.26	0.4	1409	[11]
Mesoporous activated carbon fibers	2092, 1.37	0.4	470	[65]
SACs	2729, 1.53	1.0	833	This work

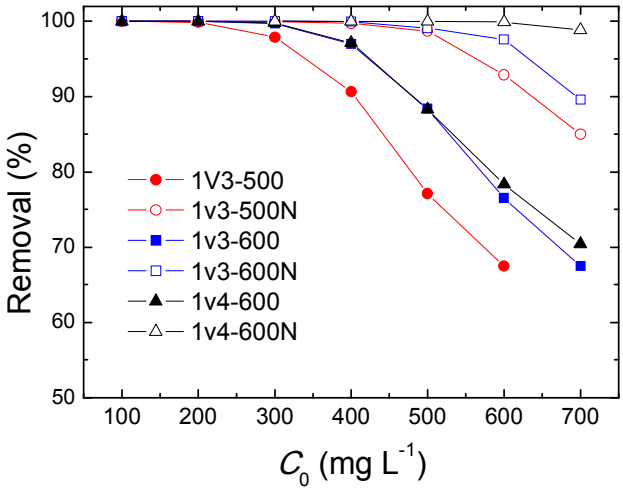

Fig. 4. RB removal efficiencies by the SACs adsorbents from solutions with varied initial RB concentrations at a dosage of 1 g L^{-1}.

The kinetics of RB adsorption on the SACs was studied on samples 1v3-500, 1v3-500N, 1v3-600 and 1v3-600N, using a RB solution with initial concentration of 400 mg L^{-1}. As shown in Fig. 5a, the adsorption of RB on 1v3-500N and 1v3-600N

reached equilibrium within 120 min, whereas a complete constant adsorption on 1v3-500 and 1v3-600 was still not achieved till 720 min. This revealed that the base leached samples exhibited obviously quicker RB adsorption than the unleached ones due to their much improved surface areas. The kinetics data was fitted to pseudo-second-order model following eq. 5 [66].

$$t/q_t=1/(k_3q_e^2)+t/q_e \quad (5)$$

where q_t is the adsorption capacity (mg g^{-1}) at time t, q_e is the adsorption capacity (mg g^{-1}) at equilibrium, k_3 is the initial adsorption rate (10^{-3} min^{-1}) for the pseudo-second-order kinetic model. The kinetic parameters obtained from the slopes and intercepts of the linearized plot of t/q_t to t are listed in Table 4. As one can judge from the data that, RB adsorption on the prepared SACs can be well described by a pseudo-second-order kinetic model as the fitting had resulted in very high correlation coefficients of all above 0.999 and good agreement between the calculated values of q_e with the experimental data. That was to say that the RB molecular was adsorbed on the surface of SACs via chemical interactions such as ionic or covalent bond.

The intra-particle diffusion model was used to analyze the kinetics data of RB adsorption on the two samples 1v3-600 and 1v3-600N, as shown in Fig. 5b [67]. It is clear that the adsorption processes of both samples can be roughly divided into three steps, as indicated by the guide lines for each portion [68]. The first portion is attributed to the diffusion of RB molecular through solution to the external surface of the adsorbent. This is a fast process that mainly depends on the surface area of the adsorbent. The second portion is attributed to the intra-particle diffusion, which is the

rate-limiting stage. In the third stage the intra-particle diffusion starts to slow down and an adsorption/desorption equilibrium is established [69]. As can be seen from the figure, the base leached sample exhibits obviously faster adsorption kinetics at the initial adsorption stage than the unleached one due to its much higher surface area. In the second and third stages, the sample 1v3-600N also shows shorter rate-limiting period for the adsorption and earlier acquirement of adsorption equilibrium than 1v3-600. This indicates that though the pore sizes of the base leached samples are not large enough to facilitate the intra-particle diffusion of the bulky RB molecular, the high pore volume has indeed enhanced the adsorption capability.

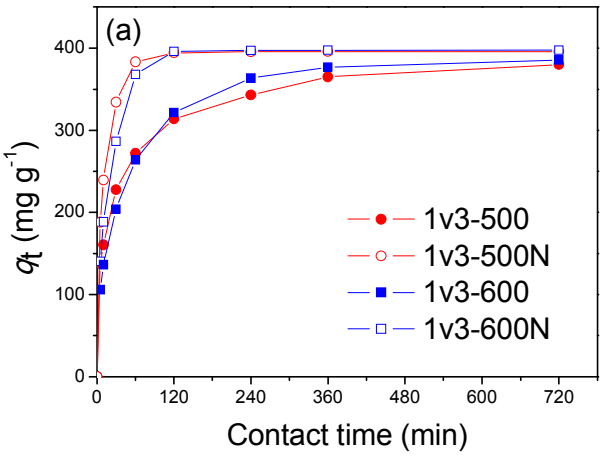

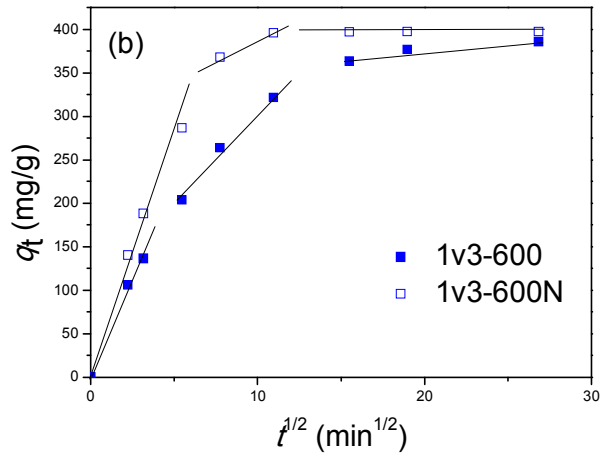

Fig. 5. The adsorption kinetics of RB on the selected SACs before and after base leaching (a) and the plots based on the intra-particle diffusion model (b).

Table 4. Kinetic parameters and constants for the pseudo-second-order fitting of the experimental data.

Adsorbent	$q_{e,exp}$ (mg g^{-1})	k_3 (10^{-3} min^{-1})	$q_{e,cal.}$(mg g^{-1})	R^2
1v3-500	380.0	0.12	387.6	0.999
1v3-500N	395.7	0.61	398.4	1
1v3-600	385.8	0.11	398.4	0.999
1v3-600N	397.5	0.33	403.2	1

The RB molecular possesses a planar structure with dimensions of 1.59×1.18×0.56 nm [61]. Such a middle-size bulky dye molecular is difficult to penetrate into the pores smaller than 2 nm during adsorption, which limits the adsorption capacity of microporosity dominant activated carbons [58]. However, despite of the high portion of micropore volume in the total pore volume of the prepared SACs (see Table 1), the adsorption capacities of RB were quite surprising. One major reason to account for this high RB adsorption capacity should be the high surface areas and large pore volumes of the SACs, especially for the base leached samples. Another plausible explanation might lie in the more accessible interpenetrated pores with sizes mostly centering at around 2 nm as were produced by extraction of boron and subsequent BPO_4 removal, similar to the secondary mesopores generated in mesoporous silica - carbon composite (MPSC)

produced by etching silica inside the pore walls [61]. Such interpenetrated pores might be accessible to RB molecular and the capillary force inside these pores had facilitated the mass transfer of dyes, which led to additional RB adsorption in these small mesopores.

4. Conclusion

Highly porous spherical activated carbons were prepared by phosphoric acid activation of boron incorporated phenolic resin spheres synthesized by a modified Stöber method followed by removal of the in situ formed BPO_4 clusters with base leaching. By alternating the impregnation ratios of phosphoric acid to the polymer spheres and activation temperatures, SACs with a surface area of 2729 $m^2 g^{-1}$ and a total pore volume of 1.529 $cm^3 g^{-1}$ were obtained, which exhibited extremely high adsorption capability towards bulky rhodamine B molecular from aqueous solutions. Analysis of the adsorption isotherms and kinetics revealed that RB adsorption on the SACs could be well described by Langmuir isotherm model and pseudo-second-order kinetic model, respectively, indicating that the adsorption occurred by formation of monolayer RB molecular on the surface of the SACs possibly via chemical interactions such as ionic or covalent bonds. Keeping in mind the variety of the elements and also the tunable amounts of them that can be pre-embedded into the polymeric precursors and extracted out by chemical activating reagents, the process reported in this work may be extended to produce SACs with controlled surface areas and pore volumes as well as pore size distributions according to the requirements of different applications.

Acknowledgements

The authors thank Drs. Xiaodan Yang and Yilai Jiao for the measurements of N_2 adsorption/desorption isotherms. C. Jiang thanks the financial support of Fujian province based on a "Minjiang Scholarship" program.

References

[1] H. Marsh, and F.R. Reinoso, Activated carbon, Elsevier, 2006.

[2] Q. Wang, X. Liang, W. Qiao, C. Liu, X. Liu, L. Zhan, and L. Ling, *Fuel Process. Technol.*, **90**, 381, (2009).

[3] A.J. Romero-Anaya, M. Ouzzine, M.A. Lillo-Ródenas, and A. Linares-Solano, *Carbon*, **68**, 296, (2014).

[4] L. Guo, J. Zhang, Q. He, L. Zhang, J. Zhao, Z. Zhu, W. Wu, J. Zhang, and J. Shi, *Chem. Commun.*, **46**, 7127, (2010).

[5] M. Ouzzine, A.J. Romero-Anaya, M.A. Lillo-Ródenas, and A. Linares-Solano, *Carbon*, **67**, 104, (2014).

[6] D.Y. Zhang, Z.F. Ma, G.X. Wang, J. Chen, G.C. Wallace, and H.K. Liu, *Catal. Lett.*, **122**, 111, (2007).

[7] J. Cheng, Y. Wang, C. Teng, Y. Shang, L. Ren, and B. Jiang, *Chem. Eng. J.*, **242**, 285, (2014).

[8] N.P. Wickramaratne, and M. Jaroniec, *ACS Appl. Mat. Interfaces*, **5**, 1849, (2013).

[9] J. Liu, S.Z. Qiao, H. Liu, J. Chen, A. Orpe, D. Zhao, and G.Q.M. Lu, *Angewandte Chemie International Edition*, **50**, 5947, (2011).

[10] H. Abe, R. Morikawa, and M. Otsuka, *Colloids Surf. B*, **103**, 538, (2013).

[11] B. Chang, D. Guan, Y. Tian, Z. Yang, and X. Dong, *J. Hazard. Mater.*, **262**, 256, (2013).

[12] A.J. Romero-Anaya, M.A. Lillo-Ródenas, and A. Linares-Solano, *Carbon*, **77**, 616, (2014).

[13] W. Li, D. Chen, Z. Li, Y. Shi, Y. Wan, J. Huang, J. Yang, D. Zhao, and Z. Jiang, *Electrochem. Commun.*, **9**, 569, (2007).

[14] S. Zhao, C.Y. Wang, M.M. Chen, J. Wang, and Z.Q. Shi, *J. Phys. Chem. Solids*, **70**,

1256, (2009).

[15] Y. Fan, X. Yang, B. Zhu, P.-F. Liu, and H.-T. Lu, *J. Power Sources*, **268**, 584, (2014).

[16] P. Zhang, Z.A. Qiao, and S. Dai, *Chem. Commun.*, **51**, 9246, (2015).

[17] A.A. Deshmukh, S.D. Mhlanga, and N.J. Coville, *Materials Science and Engineering: R: Reports*, **70**, 1, (2010).

[18] J. Qiu, Y. Li, Y. Wang, C. Liang, T. Wang, and D. Wang, *Carbon*, **41**, 767, (2003).

[19] S.-H. Yoon, Y.-D. Park, and I. Mochida, *Carbon*, **30**, 781, (1992).

[20] J.B. Yang, L.C. Ling, L. Liu, F.Y. Kang, Z.H. Huang, and H. Wu, *Carbon*, **40**, 911, (2002).

[21] Y. Liu, K. Li, and G. Sun, *J. Phys. Chem. Solids*, **71**, 453, (2010).

[22] X. Du, C.Y. Wang, M.M. Chen, S. Zhao, and J. Wang, *J. Phys. Chem. Solids*, **71**, 214, (2010).

[23] N.P. Wickramaratne, and M. Jaroniec, *J. Mater. Chem. A*, **1**, 112, (2013).

[24] A. Jain, R. Balasubramanian, and M. Srinivasan, *Chem. Eng. J.*, **273**, 622, (2015).

[25] Y. Wang, R. Yang, M. Li, and Z. Zhao, *Ind. Crops Prod.*, **65**, 216, (2015).

[26] G. Pari, S. Darmawan, and B. Prihandoko, *Procedia Environ. Sci.*, **20**, 342, (2014).

[27] M. Sevilla, and A.B. Fuertes, *Carbon*, **47**, 2281, (2009).

[28] Z.L. Xie, R.J. White, J. Weber, A. Taubert, and M.M. Titirici, *J. Mater. Chem.*, **21**, 7434, (2011).

[29] M. Zhang, H. Yang, Y. Liu, X. Sun, D. Zhang, and D. Xue, *Carbon*, **50**, 2155, (2012).

[30] C.F. Zhang, K.B. Hatzell, M. Boota, B. Dyatkin, M. Beidaghi, D.H. Long, W.M. Qiao, E.C. Kumbur, and Y. Gogotsi, *Carbon*, **77**, 155, (2014).

[31] J. Ludwinowicz, and M. Jaroniec, *Carbon*, **82**, 297, (2015).

[32] D.L. Wang, M.M. Chen, C.Y. Wang, J. Bai, and J.M. Zheng, *Mater. Lett.*, **65**, 1069, (2011).

[33] B. Friedel, and S. Greulich-Weber, *Small*, **2**, 859, (2006).

[34] B. Weber, W. Bremser, and K. Hiltrop, *Prog. Org. Coat.*, **64**, 150, (2009).

[35] Q. Sun, X.Q. Zhang, F. Han, W.C. Li, and A.H. Lu, *J. Mater. Chem.*, **22**, 17049,

(2012).

[36] J. Liu, S.Z. Qiao, H. Liu, J. Chen, A. Orpe, D. Zhao, and G.Q. Lu, *Angew. Chem. Int. Ed.*, **50**, 5947, (2011).

[37] M. Molina-Sabio, and F. Rodríguez-Reinoso, *Colloids Surf., A*, **241**, 15, (2004).

[38] Z.M. Zou, Y.L. Tang, C.H. Jiang, and J.S. Zhang, *J. Environ. Chem. Eng.*, **3**, 898, (2015).

[39] A.A. Attia, B.S. Girgis, and S.A. Khedr, *J. Chem. Technol. Biotechnol.*, **78**, 611, (2003).

[40] G. Mezohegyi, F.P. van der Zee, J. Font, A. Fortuny, and A. Fabregat, *J. Environ. Manage.*, **102**, 148, (2012).

[41] G. Wang, L. Zhang, and J. Zhang, *Chem. Soc. Rev.*, **41**, 797, (2012).

[42] N. Fechler, S.-A. Wohlgemuth, P. Jäker, and M. Antonietti, *J. Mater. Chem. A*, **1**, 9418, (2013).

[43] N. Fechler, T.-P. Fellinger, and M. Antonietti, *Adv. Mater.*, **25**, 75, (2013).

[44] N. Bhandari, R. Dua, L. Estevez, R. Sahore, and E.P. Giannelis, *Carbon*, **87**, 29, (2015).

[45] X. Liu, and M. Antonietti, *Carbon*, **69**, 460, (2014).

[46] X. Deng, B. Zhao, L. Zhu, and Z. Shao, *Carbon*, **93**, 48, (2015).

[47] P. Kuhn, A. Forget, D. Su, A. Thomas, and M. Antonietti, *J. Am. Chem. Soc.*, **130**, 13333, (2008).

[48] P. Kuhn, M. Antonietti, and A. Thomas, *Angew. Chem. Int. Ed.*, **47**, 3450, (2008).

[49] A. Muthukrishnan, Y. Nabae, C.W. Chang, T. Okajima, and T. Ohsaka, *Catal. Sci. Technol.*, **5**, 1764, (2015).

[50] R. Saraswat, N. Talreja, D. Deva, N. Sankararamakrishnan, A. Sharma, and N. Verma, *Chem. Eng. J.*, **197**, 250, (2012).

[51] X. Zhao, A. Wang, J. Yan, G. Sun, L. Sun, and T. Zhang, *Chem. Mater.*, **22**, 5463, (2010).

[52] S.J. Gregg, K.S.W. Sing, and H.W. Salzberg, *J. Electrochem. Soc.*, **114**, 279C, (1967).

[53] E.P. Barrett, L.G. Joyner, and P.P. Halenda, *J. Am. Chem. Soc.*, **73**, 373, (1951).

[54] B.H. Plesner, and K. Hansen, *Carcinogenesis*, **4**, 457, (1983).

[55] J. Rouquerol, D. Avnir, D.H. Everett, C. Fairbridge, M. Haynes, N. Pernicone, J.D.F. Ramsay, K.S.W. Sing, and K.K. Unger, Guidelines for the Characterization of Porous Solids, in: F.R.-R.K.S.W.S. J. Rouquerol, K.K. Unger (Eds.) Stud. Surf. Sci. Catal., Elsevier, 1994, pp. 1.

[56] A. Mehrdad, and R. Hashemzadeh, *Ultrason. Sonochem.*, **17**, 168, (2010).

[57] S. Sachdeva, and A. Kumar, *J. Membr. Sci.*, **329**, 2, (2009).

[58] M. Mohammadi, A.J. Hassani, A.R. Mohamed, and G.D. Najafpour, *J. Chem. Eng. Data*, **55**, 5777, (2010).

[59] I. Langmuir, *J. Am. Chem. Soc.*, **40**, 1361, (1918).

[60] Z. Hu, L. Lei, Y. Li, and Y. Ni, *Sep. Purif. Technol.*, **31**, 13, (2003).

[61] X. Zhuang, Y. Wan, C. Feng, Y. Shen, and D. Zhao, *Chem. Mater.*, **21**, 706, (2009).

[62] L. Li, S. Liu, and T. Zhu, *J. Environ. Sci.*, **22**, 1273, (2010).

[63] M.E. Fernandez, G.V. Nunell, P.R. Bonelli, and A.L. Cukierman, *Ind. Crops Prod.*, **62**, 437, (2014).

[64] L. Ding, B. Zou, W. Gao, Q. Liu, Z. Wang, Y. Guo, X. Wang, and Y. Liu, *Colloids Surf., A*, **446**, 1, (2014).

[65] Y. Dong, H. Lin, Q. Jin, L. Li, D. Wang, D. Zhou, and F. Qu, *J. Mater. Chem. A*, **1**, 7391, (2013).

[66] Y.S. Ho, and G. McKay, *Process Biochem.*, **34**, 451, (1999).

[67] T.W. Weber, and R.K. Chakravorti, *AlChE J.*, **20**, 228, (1974).

[68] F.C. Wu, R.L. Tseng, and R.S. Juang, *Environ. Technol.*, **22**, 205, (2001).

[69] Z. Al-Othman, R. Ali, and M. Naushad, *Chem. Eng. J.*, **184**, 238, (2012).

Sentence for graphical abstract:

Highly porous spherical activated carbons were synthesized by combination of H_3PO_4 activation and boron templating for efficient RB adsorption.

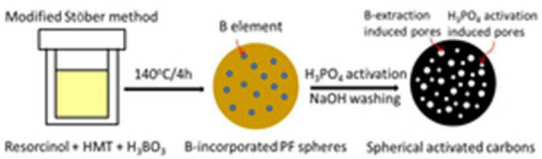

23x6mm (300 x 300 DPI)